FIP effect measurements in the off-limb corona observed by SUMER on SOHO

A. Mohan[1], E. Landi[2], and B.N. Dwivedi[1,2]

[1] Banaras Hindu University, Institute of Technology, Department of Applied Physics, Varanasi 221005, India
[2] Max-Planck-Institut für Aeronomie, 37191 Katlenburg-Lindau, Germany

Abstract. Systematic differences between elemental abundances in the corona and in the photosphere have been long acknowledged in the Sun; these abundance anomalies are correlated with the first ionization potentials (FIPs) of the elements. This correlation is called FIP effect. Using spectra obtained from the SUMER (Solar Ultraviolet Measurements of Emitted Radiation) spectrograph on the spacecraft SOHO (Solar and Heliospheric Observatory), we investigate electron density, temperature and the abundance anomalies in the off-limb solar corona. In particular, we present the behaviour of the solar FIP effect with height above an active region observed at the solar limb, with K/Ar, Si/Ar and S/Ar ratios of lines present in the recorded UV spectra.

We find that the K FIP bias seems to be higher than for the other low-FIP elements, and that the Si and K FIP biases are dependent on the distance from the photosphere. Studying the Ne/Mg line ratio in the active region, we also investigate the presence of the FIP effect in active region structures.

Key words: Sun: abundances – Sun: atmosphere – Sun: UV radiation

1. Introduction

The knowledge of the composition of the corona is an important key to our understanding of the physical processes in the solar atmosphere. The coronal elemental abundances can help to investigate the mechanisms that transport, accelerate and heat the solar coronal plasma and wind. The composition of the corona must also be known in order to interpret observations of coronal emission spectra. Elements' relative abundances must be known also to determine temperatures from the intensity ratios of the coronal lines of different elements, while the absolute abundances must be known to determine emission measure and radiation losses. Obviously, elemental abundances are among the most fundamental sets of parameters in the solar and stellar atmospheres. Extensive research regarding the abundances of elements in the solar atmosphere has been reviewed by Feldman (1992), and an update on the most recent results can be found in the recent review by Feldman & Laming (2000).

Send offprint requests to: E. Landi (enricol@arcetri.astro.it)

The status of coronal abundances relative to hydrogen is not entirely settled. There is a significant body of evidence that abundances are correlated with the first ionization potential, giving rise to the so-called FIP effect. This effect consists of systematic differences between photospheric and coronal element abundances. The latter show enhancements of a factor around 4 in the so-called low-FIP elements (FIP ≤ 10 eV), while abundances for the high-FIP elements (FIP > 10 eV) remain constant between the photosphere and the corona. So far, no theoretical model has been able to satisfactorily explain this effect.

Dwivedi et al. (1997, 1999a) carried out an observing sequence based on a theoretical study by Dwivedi & Mohan (1995), with intercombination and forbidden Ne VI and Mg VI lines, which are formed at essentially the same temperature (4×10^5 K), according to Arnaud & Rothenflug (1985). The FIPs of Ne and Mg are 21.6 and 7.6 eV, respectively: they form a low-FIP/high-FIP pair. This study provided new observational facts in transition region emission lines (Dwivedi et al. 1999a,b). In the present paper, we extend this investigation taking account of other low-FIP/high-FIP pairs such as K/Ar, Si/Ar and S/Ar present in the spectra. The use of the recently identified K XIII line at 994.58 Å (Mohan et al. 2000) allows us to investigate the amount of FIP bias also for the very low-FIP element K (FIP = 4.3 eV), so that it is possible to investigate whether the FIP bias of the elements with FIP ≤ 10 eV is constant or depends on the FIP value of each element, as suggested by Feldman & Laming 2000.

The FIP bias of the S, Si and K elements is also investigated as a function of the height above the photosphere. Also, the Mg/Ne ratio is re-examined and correlated with structures in the field of view.

We briefly describe the observations in Sect. 2 and plasma diagnostics in Sect. 3. Density and temperature measurements are discussed in Sect. 4. We present the relative element abundances in Sect. 5 and discuss them in Sect. 6.

2. Instrument and observations

The observations were made with the SUMER spectrograph on 1996 June 20 above the active region NOAA 7974 at the solar east limb, starting at 20:11 UT. Fig. 1 shows the position and extension of the SUMER raster superimposed on the He II 304 Å

raster direction
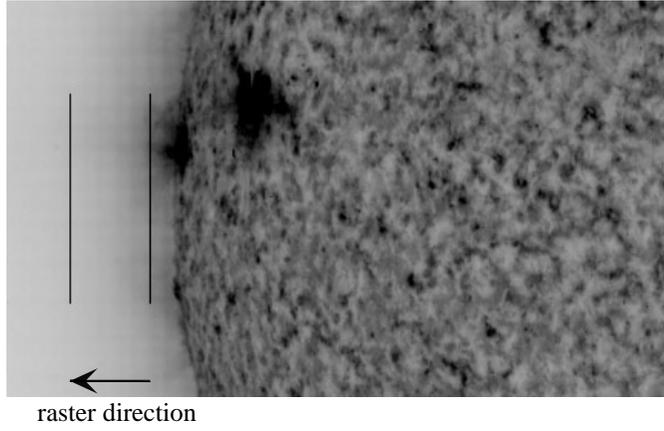
Fig. 1. SUMER raster superimposed on a section of the He II 304 Å EIT image taken at 19:41 UT, showing the active region NOAA 7974 on the limb and its neighbour NOAA 7973 in photonegative representation. (Courtesy, EIT/SOHO consortium)

Table 1. Spectral lines considered in the present work. The Si XI line is observed in second order.

Ion	Wvl. (Å)	Transition
Ne VI	992.73	$2s^2 2p\ ^2P_{1/2} - 2s2p^2\ ^4P_{3/2}$
K XIII	994.58	$2s^2 2p^3\ ^4S_{3/2} - 2s^2 2p^3\ ^2D_{3/2}$
Ne VI	997.14	$2s^2 2p\ ^2P_{1/2} - 2s2p^2\ ^4P_{1/2}$
Ne VI	999.26	$2s^2 2p\ ^2P_{3/2} - 2s2p^2\ ^4P_{5/2}$
Ne VI	1005.70	$2s^2 2p\ ^2P_{3/2} - 2s2p^2\ ^4P_{3/2}$
Ne VI	1010.25	$2s^2 2p\ ^2P_{3/2} - 2s2p^2\ ^4P_{1/2}$
Ar XII	1018.87	$2s^2 2p^3\ ^4S_{3/2} - 2s^2 2p^3\ ^2D_{5/2}$
Mg VII	1189.85	$2s^2 2p^2\ ^3P_1 - 2s^2 2p^2\ ^1S_0$
Mg VI	1190.10	$2s^2 2p^3\ ^4S_{3/2} - 2s^2 2p^3\ ^2P_{3/2}$
Mg VI	1191.64	$2s^2 2p^3\ ^4S_{3/2} - 2s^2 2p^3\ ^2P_{1/2}$
S X	1196.25	$2s^2 2p^3\ ^4S_{3/2} - 2s^2 2p^3\ ^2D_{5/2}$
Si XI	604.17	$2s2p\ ^1P_1 - 2p^2\ ^1D_2$
S X	1213.00	$2s^2 2p^3\ ^4S_{3/2} - 2s^2 2p^3\ ^2D_{3/2}$

image of the eastern limb of the Sun taken at 19:41 UT with the EIT ultraviolet imager (Delaboudiniere et al. 1995).

A full description of SUMER and its performance are given in Wilhelm et al. (1995, 1997) and Lemaire et al. (1997). The instrument is an ultraviolet telescope and spectrometer with a wavelength resolution element of 42–44 mÅ over the range 800–1610 Å (in first order). The spatial resolution is about 1" in the N-S direction, while in the E-W direction it depends on the slit width. In the observations analyzed in the present work a slit size of 4"x300" was used. The raster started 40" off-limb, above the position of the bright He II protrusion seen in the EIT image, and the slit was stepped eastward for 133". At each position, two 40 Å wide spectra were obtained, one centered on the Ne VI 999 Å line, and the other on the Mg VI 1191 Å line. The integration time per spectrum was increased exponentially with position from 250 s at 40" to 867 s at 173". The total raster time was about 10 hr. The lines used in the present study are reported in Table 1.

The observations analyzed in the present work include both plasma from active region structures and outside these structures. Fig. 2 shows the intensity maps obtained from S X and Mg VI lines. Mg VI shows a highly structured behaviour, indicating that this ion is present only inside in a relatively cool structured area belonging to the active region at the limb. Outside this area the residual Mg VI emission is mainly due to scattered light. S X presents a fairly uniform map with no signature of the active region.

We will refer to the low temperature plasma inside the structures as "prominence" plasma, and to the hotter coronal plasma as "active region corona". In the present work these two plasmas have been analysed separately.

3. Plasma diagnostics

Without a knowledge of the density, temperature, and elemental abundances in astrophysical plasmas, almost nothing can be said regarding the physical processes taking place in them. Thus,

a considerable effort has been made in the past years in developing diagnostic techniques to infer plasma temperature, density, and elemental abundances for solar and other astrophysical plasmas, especially by means of optically thin emission-line spectra (e.g., Dwivedi 1994; Mason & Monsignori-Fossi 1994, and references therein). A fundamental property of hot solar plasmas is their inhomogeneity. The emergent intensities of spectral lines from optically thin plasmas are determined by integrals along the line of sight through the plasma. Spectroscopic diagnostics of the temperature and density structure of hot optically thin plasmas using emission-line intensities is usually described in two ways. The line-ratio method uses an observed line intensity ratio to determine density or temperature from theoretical density or temperature-sensitive line-ratio curves, calculated taking account of physical processes for the formation of lines, in the assumption that both lines are emitted by the same plasma volume. The line-ratio method is stable, leading to well-defined values of T or N_e, but in realistic cases of inhomogeneous plasmas the results are hard to interpret. The more general "differential emission measure" (*DEM*) method (e.g., Mason & Monsignori-Fossi 1994) recognizes that observed plasmas are better described by distributions of temperature or density along the line of sight, and poses this problem in inverse form. Derivation of *DEM* functions, while more generally acceptable, is unstable to noise and errors in spectral and atomic data. The exact relationship between the two approaches has never been explored in depth, although particular situations were discussed by Brown et al. (1991). The mathematical relationship between these two approaches has recently been reported by McIntosh et al. (1998).

However, since off-limb plasma outside active regions has been found to be nearly isothermal (Feldman et al. 1998), the *DEM* approach loses its meaning, and a line ratio approach is sufficient for our purposes. However, the presence of many plasma structures in the field of view complicates the analysis for the cooler lines in our dataset. Since SUMER lacks the capability of spatially resolving the individual structures, we have to
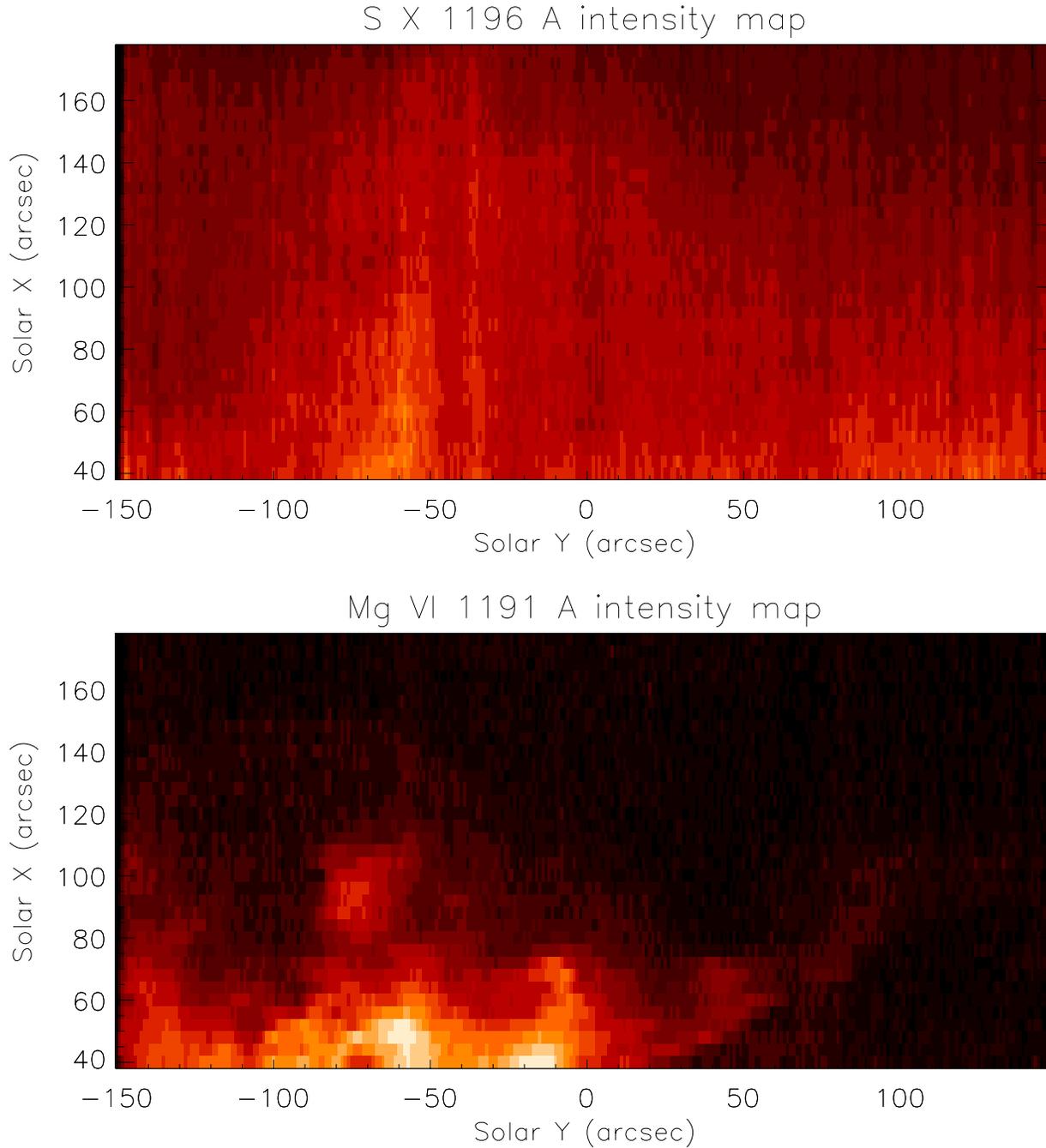
Fig. 2. S X 1196 Å (top) and Mg VI 1191 Å (bottom) intensity maps of the emitting region.

consider the results obtained with the Mg/Ne ratios as averages over several different structures.

The power P per unit volume (in energy units) emitted in an optically thin spectral line emanating from an upper level (j) to a lower level (i) is given by

$$P_{ij} = h\nu_{ij}A_{ij}N_j(X^{+m}) \tag{1}$$

where A_{ij} is the transition probability, $N_j(X^{+m})$ is the population of the upper level j of the ion X^{+m}. $N_j(X^{+m})$ can be further parametrized as

$$N_j(X^{+m}) = \frac{N_j(X^{+m})}{N(X^{+m})} \frac{N(X^{+m})}{N(X)} \frac{N(X)}{N(H)} \frac{N(H)}{N_e} N_e \tag{2}$$

where $\frac{N_j(X^{+m})}{N(X^{+m})}$ is the relative upper level population, $\frac{N(X^{+m})}{N(X)}$ is the ion fraction of the ion X^{+m}, $\frac{N(X)}{N(H)}$ is the abundance of the element relative to hydrogen, which varies in different astrophysical plasmas and also in different solar features, $\frac{N(H)}{N_e}$ is usually assumed to be around 0.8 for a fully ionized plasma.

Combining Eqs. (1) and (2), we can write

$$P_{ij} = 0.8\, h\nu_{ij} A_{ij}\, \frac{N_j(X^{+m})}{N(X^{+m})}\, \frac{N(X^{+m})}{N(X)}\, \frac{N(X)}{N(H)}\, N_e \qquad (3)$$

where $\frac{N_j(X^{+m})}{N(X^{+m})}$ is evaluated at the plasma electron density and temperature, and $\frac{N(X^{+m})}{N(X)}$ is evaluated at the plasma temperature.

In low-density plasmas, the collisional excitation processes are generally faster than ionization and recombination timescales, and therefore the collisional excitation is dominant over ionization and recombination in populating excited states. The low-lying level populations can then be treated separately from the ionization and recombination processes. The number density population of level j is calculated by solving the statistical equilibrium equations for a number of low-lying levels, taking account of all the important collisional and radiative excitation and deexcitation mechanisms.

In order to obtain relative abundances of two elements X and Y, ratios of spectral line intensities from the two elements are used. The line intensity ratio R of two lines is given by

$$R = \frac{\lambda_{kl}}{\lambda_{ij}}\, \frac{A_{ij}}{A_{kl}}\, \frac{\frac{N_j(X^{+m})}{N(X^{+m})}\, \frac{N(X^{+m})}{N(X)}}{\frac{N_l(Y^{+m})}{N(Y^{+m})}\, \frac{N(Y^{+m})}{N(Y)}}\, \frac{N(X)}{N(Y)} \qquad (4)$$

If the intensities of the two lines have a similar temperature dependence, then the lines are presumably formed in the same plasma volume and at the same density. For determining the relative element abundance between X and Y, we can then compute a theoretical line intensity ratio assuming equal abundances for X and Y, and subsequently deduce $\frac{N(X)}{N(Y)}$ from the observed line intensity ratio R_{obs}.

Theoretical line ratios have been computed using the CHIANTI database (Dere et al. 1997; Landi et al. 1999) and the density and temperature values measured from the observations, assuming unity elemental abundances. Unless otherwise specified, ion fractions come from Mazzotta et al. (1998).

4. Density and temperature measurements

The observed plasma clearly has two components, one with complex structures in the active region (the "prominence" plasma), and the other outside these structures ("active region corona"), as shown in Fig. 2. Thus we present density and temperature measurements carried out in both plasmas.

4.1. Prominence plasma

The temperature and density maps of the cooler plasma inside the active region structures is displayed in Fig. 3, where also the Ne VI 1005 Å intensity map is shown. The intensity, density and temperature for the plasma observed at solar X=45" are shown in Fig. 4, where the uncertainties of each measurements are also reported. It is important to note that Ne VI and Mg VI emission outside the bright structures in Fig. 3 is due mainly

to instrument-scattered light. Plasma diagnostics has not been carried out at these positions.

Making use of density-sensitive 1190/1191 Mg VI line ratio, we find that the electron density (log value) varies from 9.0 to 9.7 (N_e in cm^{-3}) inside the bright structures. Uncertainties at each pixel position are 0.15 dex. These are given by the combination of the uncertainties in the fitted line profile parameters and in the SUMER intensity calibration. The random fluctuation of the measured density between 10" and 40" in Fig. 3 are probably due to the strong contribution of the scattered light to line intensities and to the weakness of true line emission.

The temperature, determined via the Mg VII/Mg VI 1189/1191 line ratio, is also displayed in Fig. 3. It is possible to see that, where the Mg VI and Ne VI emission is strongest, the ratio is almost constant, with a value of about 5–6$\times 10^5$ K. Outside the brightest positions, the ratio increases and shows a greater noise, due to the weakness of the diagnostic lines and to the increasing importance of the scattered light component to line intensity. The theoretical Mg VII/Mg VI ratio has been calculated in each pixel adopting the measured density value, to take into account the density sensitivity of the Mg VI 1191.64 Å line. The prominence plasma is thus relatively cooler and denser compared to the surrounding unstructured plasma (see next section).

The pixel-to-pixel variation of the electron density suggests the presence of many unresolved plasma structures, with very similar electron temperatures and different density.

It is interesting to note that the use of different ion fraction datasets to calculate the Mg VII/Mg VI theoretical ratio does not affect the results significantly, although some difference can be seen between ion fractions coming from different sources (Fig. 5). This is consistent with the results reported by Allen et al. (2000).

4.2. Active region corona

Temperature and density for the off-limb plasma are displayed in Fig. 6. We have used density-sensitive 1196/1213 S X line ratio to determine N_e outside the structure. When the plasma density is fairly low, we must take account of photoexcitation of ground levels by photospheric radiation in calculating level populations for many ions. There is a critical density below which ground levels' populations are affected by such a process. In our dataset N_e is sufficiently low to let photoexcitation play an important role for S X density diagnostics. Using CHIANTI and taking account of this process, the inferred log N_e values as a function of height are shown in Fig. 6 (top). Uncertainties increase with height, and the last 5 density values are only an estimate of an upper limit, due also to the "flattening" of the theoretical ratio. Apart from the very last ratios, these values lie more or less on a straight line as a function of height.

We also measured electron temperature T outside the structure from Ar XII 1018/S X (1196+1213) line ratio as a function of height. It is to be noted here that such a measurement could be biased to any problem in the relative Ar/S abundance. Argon is a high-FIP element while sulfur is just at the border (its FIP

Ne VI 1005 A intensity map

Temperature map

Density map

Ne VI/Mg VI abundance ratio
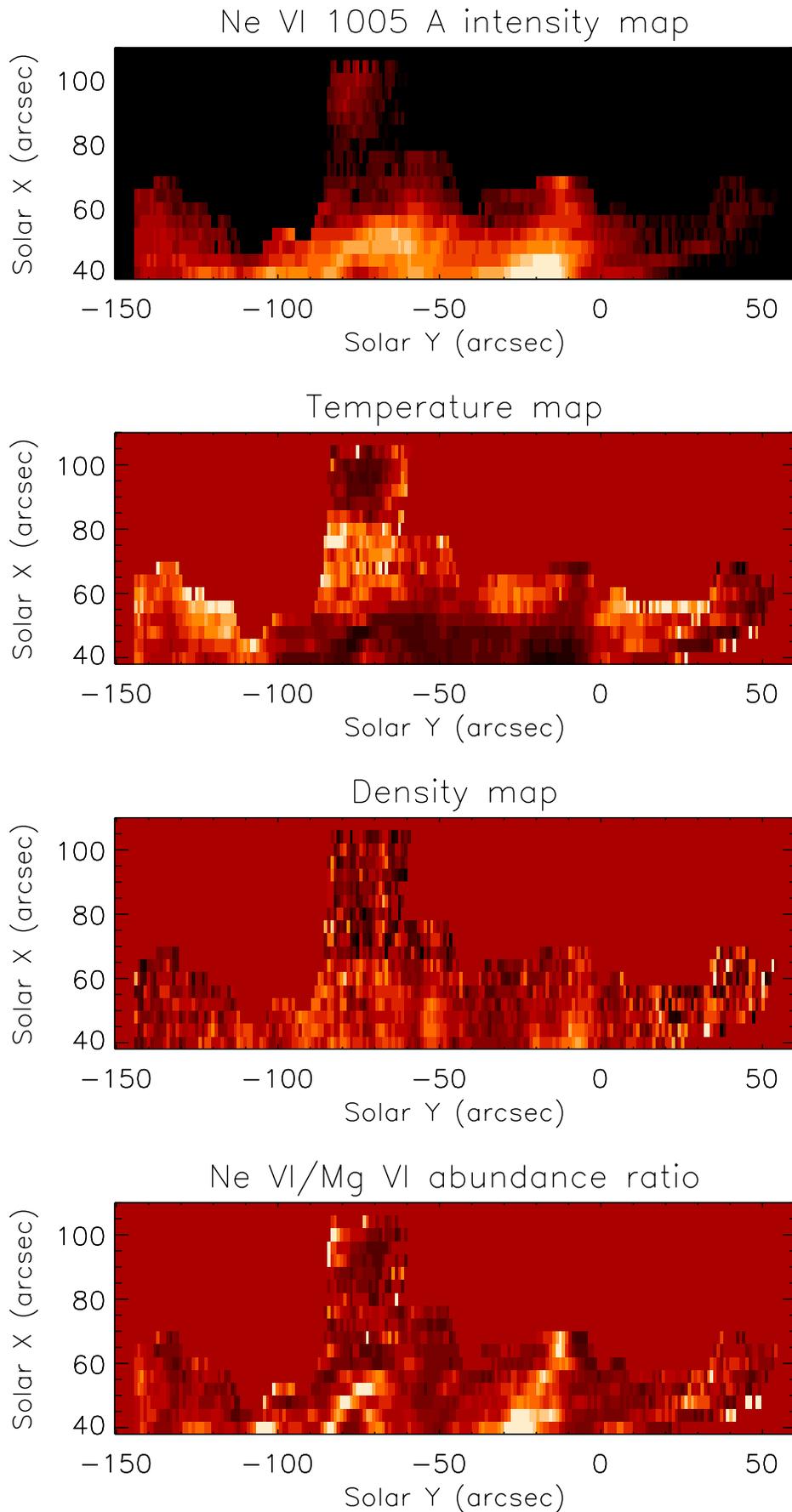
Fig. 3. Diagnostic results in the active region structures. From the top: 1 – Ne VI 1005 Å intensity map of the structures (in he black portion line intensity is due mainly to instrument-scattered light); 2 – Temperature map from the Mg VII/Mg VI line ratio; 3 – Density map from the Mg VI line ratio; 4 – Ne VI/Mg VI line ratio, yielding an estimate of the Ne/Mg abundance.
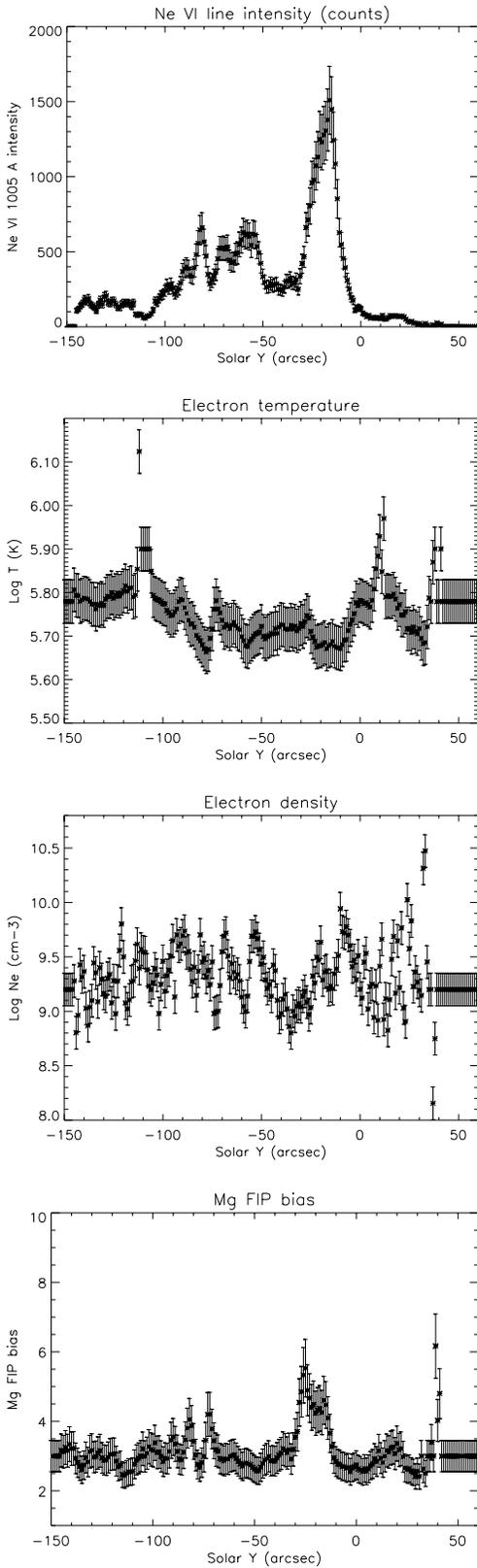
Fig. 4. Diagnostic results in the active region structures, at solar X=45''. From the top: 1 – Ne VI 1005 Å intensity 2 – Temperature from the Mg VII/Mg VI line ratio; 3 – Density from the Mg VI line ratio; 4 – Ne VI/Mg VI line ratio, yielding an estimate of the relative Ne/Mg abundance.
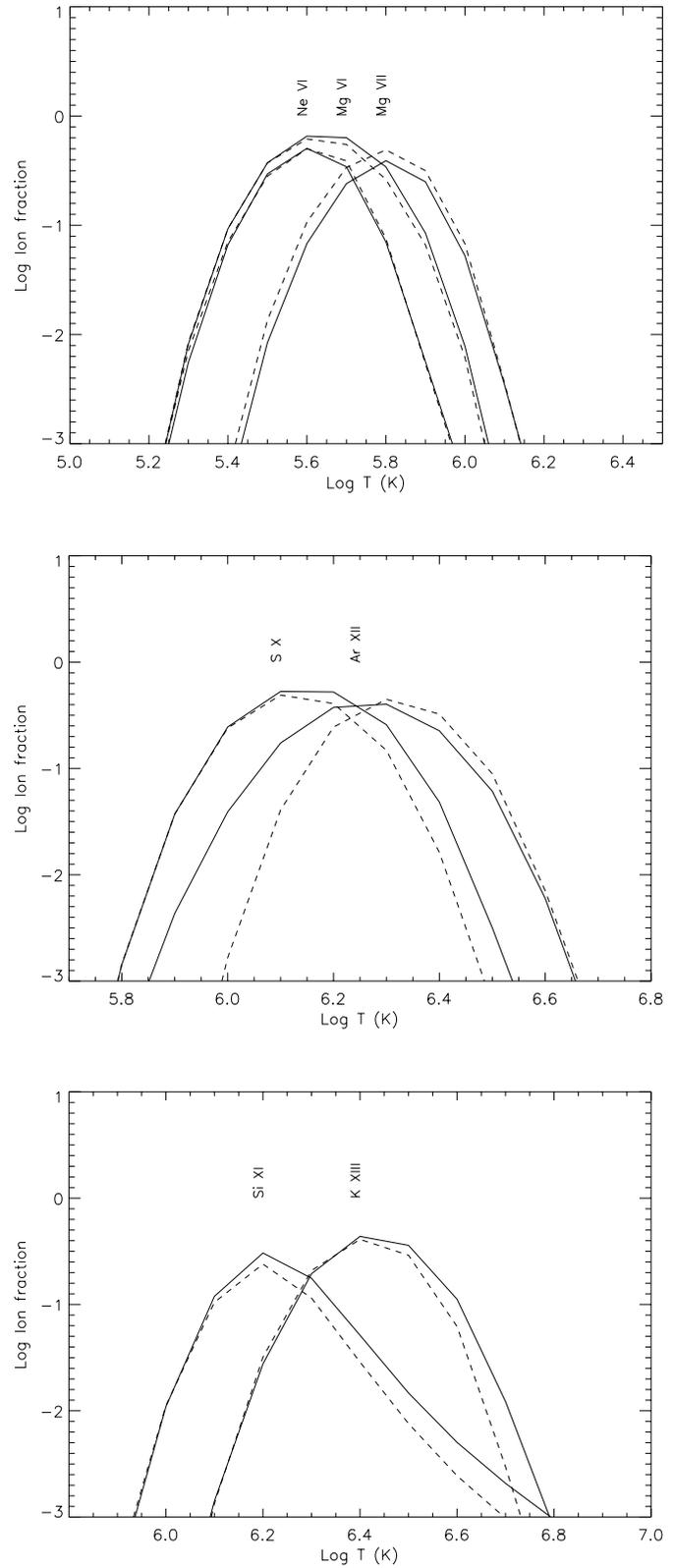
Fig. 5. Ion fraction of the ions used in the present work. **Full line**: Mazzotta et al. (1998). **Dashed line**: Arnaud & Rothenflug (1985) (Si, S, Ar), Landini & Monsignori Fossi (1991) (K).
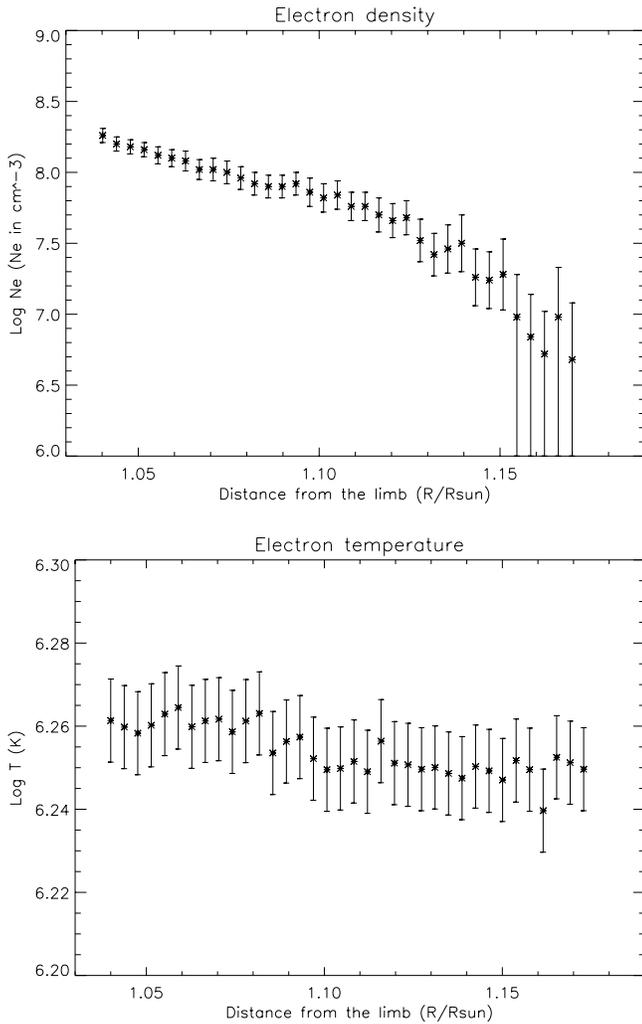
Fig. 6. Top: Density vs. height from the S X line ratio; **Bottom**: temperature versus height from the Ar XII/S X line ratio.

is 10.4 eV), so this can provide additional uncertainty to our results. However, our study has shown (see Sect. 5.2) that S/Ar abundance remains photospheric all across the field of view, so that this uncertainty should be reduced.

We find from this ratio that the electron temperature remains more or less constant with height with log T values between 6.24 and 6.26, assuming photospheric abundances. These values are slightly higher than those provided by Feldman et al. (1998) and Allen et al. (2000) in the quiet off-limb solar corona.

5. Relative element abundances

5.1. Prominence plasma

Making use of the intensity maps from Ne VI 1005.70 Å and Mg VI 1191.64 Å, we determined the Ne/Mg ratio across the whole field of view and compared it with the Ne VI 1005.70 Å intensity map, which shows the complex plasma distribution of the active region. Results are shown in Fig. 3 and, for solar X=45", in Fig. 4, where also the uncertainties are reported. It is to be noted that outside the intense central region, the Ne VI

and Mg VI intensity is mainly due to instrument-scattered light, so that the ratio has not been calculated.

The variation of the Mg/Ne relative abundance seems to be strongly correlated with the plasma structures in the emitting source. Although the instrument resolution is not enough to resolve individual structures precisely, we find that some structures with strong Ne VI and Mg VI line emission in Figs. 2 and 3 indicate a normal FIP-bias in Mg/Ne varying from 1.6 to 3.2. However, in regions with strong Mg VI and weak Ne VI line emission the FIP-bias ranges from 3.1 to 8.8.

These values show that the complex plasma structuring of the active region can have a strong effect on element abundances. Although the FIP bias is present in all the active region, its variability seem to suggest that the plasma in each individual structure might have its own peculiar composition. Such a possibility has been already suggested by a number of authors, who report abundance variations in active regions similar to ours (see for example Young & Mason 1997; Widing & Feldman 1993, 1995; Landi & Landini 1998a). Unfortunately, the lack of sufficient spatial resolution prevents a more detailed study.

It is important to note that Ne VI and Mg VI ion fraction curves (as shown in Fig. 5) are quite different. This causes the relative intensity ratio between lines of these two ions to be temperature dependent, so that it is necessary to take into account the plasma electron temperature when these two ions are used for measurements of Ne/Mg relative abundance.

5.2. Active region corona

In the unstructured, hot coronal plasma we studied the low-FIP/high-FIP pairs S/Ar, Si/Ar and K/Ar and the height dependence of their intensity ratios. The FIPs for K, Si, S and Ar are 4.3, 8.2, 10.4 and 15.8 eV respectively. We have investigated experimental S X/Ar XII, Si XI/Ar XII and K XIII/Ar XII ratios, determining the FIP variation with height in the corona outside the structures. The results are displayed in Fig. 7.

The results for the K/Ar, Si/Ar and S/Ar abundances outside the structures show different behaviours.
The coronal relative abundance of S/Ar shown in Fig. 7 (top) stays almost at its photospheric value.

Si/Ar shown in Fig. 7 (middle) varies between 18 and 26 compared to its photospheric value of 9. Thus we find a FIP factor of 2 to 3 for Si/Ar in the corona. It is interesting to note that, apart from the last three positions, the Si/Ar relative abundance seems to decrease with height. The difference is slightly greater than the uncertainties, and show that the Si abundance tends to decrease relative to the Ar value.

The case of K/Ar shown in Fig. 7 (bottom) requires some more detailed discussion.

K has a very low abundance, apart from having the lowest FIP among the elements whose coronal abundance can be determined spectroscopically. Using the relative intensity of a K XVIII/Ca XIX line ratio, observed by the Solflex X-ray spectrometer on the NRL P78-1 satellite, Doschek et al. (1985) established that the abundance ratio of K/Ca=0.10. Anders & Grevesse (1989) give a photospheric abundance ratio of
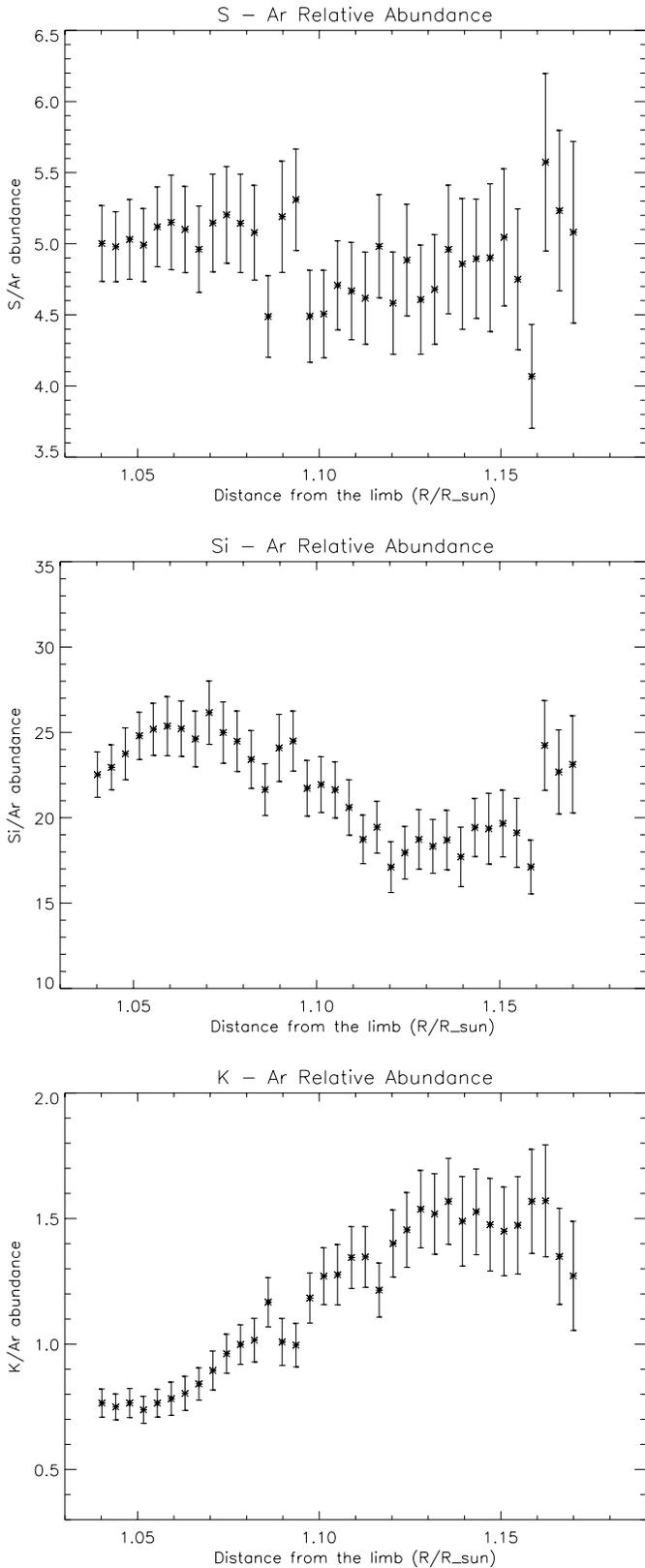
Fig. 7. S, Si and K element abundances relative to the Ar photospheric abundance.

K/Ca =0.058 which is a factor of 1.7 lower than the ratio obtained from the flare data. Using the photospheric abundance of Ca/H=2.24×10^{-6}, we get K/H=1.3×10^{-7}, which we assume as the reference K photospheric abundance. In our study we find that the K/Ar relative abundance varies from 0.7 to 1.6 in the off limb plasma, showing a clear, strong FIP bias. The values of the FIP bias varies from 16 to 36, stronger than any FIP bias result quoted in the literature.

The K XIII line belongs to the nitrogen isoelectronic sequence. The CHIANTI atomic data for this ion (Landi et al. 1999; Landi & Landini 1998b) consist of an interpolation of the old Bhatia & Mason (1980) collisional and radiative transition probabilities, and not of *ab-initio* calculations. This leaves a greater uncertainty in the calculation of the theoretical K/Ar ratio. Future CHIANTI releases will include new K transition probabilities from the calculations of Zhang & Sampson (1999), which could help in providing a more accurate value for the K FIP bias. However, it is unlikely that uncertainties in the CHIANTI data for K are larger than a factor 2, so that the K bias is still significantly greater than Si values from our work, and also than the values usually quoted in the literature for Mg, Al, Si ions.

Recently, Kink et al. (1999) report the identification of a few Si VIII and S X high excitation lines, measured using laboratory beam-foil techniques, and the SUMER quiet Sun spectral atlas taken above a quiet area outside the solar limb by Feldman et al. (1997).

The wavelength of the Si VIII $3p$ $^{4}D_{7/2}$–$3d$ $^{4}F_{9/2}$ at 994.58 Å is very close to the K XIII line measured in the present work, so that this line is expected to blend the K XIII line. Also, in the present dataset other unidentified lines are found matching the wavelengths of the Si VIII ^{4}D–^{4}F transitions reported by Kink et al. (1999), confirming the presence of the blending line at 994.58 Å.

In order to investigate the importance of the Si VIII contribution to the K XIII line, we have tried to investigate these lines. The relative intensities of these transitions, as measured in the present work, are substantially different than those reported by Kink et al. (1999), so that it is not possible to estimate the Si VIII contribution by simple line ratios with the other line of the ^{4}D–^{4}F multiplet. This is probably due to the different plasma conditions in the present dataset and in the one analyzed by Kink et al. (1999).

Theoretical estimates carried out with the HULLAC code (Klapisch 1971; Klapisch et al. 1977; Liedahl et al. 1995 – courtesy of Dr. J.M.Laming) have permitted us to estimate the theoretical emissivity of these lines under the physical conditions of the present dataset. However, HULLAC results show that Si VIII is not expected to provide significant intensity to K XIII. However, since these Si VIII transitions have very high excitation energies, the HULLAC code could underestimate their emissivity (J.M.Laming, private communications). Consequently, these results do not rule out possible blending problems, and no definitive conclusions cannot be drawn from the present dataset on the magnitude of the K FIP bias.

5.3. Uncertainties in the FIP bias measurements

In order to calculate theoretical line ratios, we need to use not only the correct N_e and T values, but also an ion fraction dataset. This parameter represents a further source of uncertainty in our FIP measurements as well as in most diagnostic techniques involving UV-EUV lines (Gianetti et al. 2000). Thus it is important to assess the uncertainties provided by the ion fractions.

We compared the FIP biases obtained adopting in turn the two most recent different ion fraction datasets available in the literature for the ions used in the present work: Mazzotta et al. (1998), and Arnaud & Rothenflug (1985) (with K from Landini & Monsignori Fossi 1991). Ion fractions are displayed in Fig. 5 for the solar ions used for spectroscopic diagnostics in the present study. Fig. 5 shows that all the ions that we are considering present differences between the two ion fraction datasets. This results in a bias to the theoretical ratio which is purely given by the ion fraction dataset used. The uncertainty ranges between 20% and 40%, and must be added to the experimental uncertainty from measured line intensities.

6. Is the FIP bias dependent on FIP value?

The FIP biases for S, Si and K measured in the present work show a different behaviour in two senses:

1. height dependence
2. magnitude of the FIP bias

The sulphur FIP bias is almost negligible, showing that S abundance is photospheric within uncertainties, and does not change with height. Si instead shows a typical FIP bias magnitude, that seems to become smaller as height increases (although the most distant three values contradict this). The change with height is $\simeq 30\%$ at maximum, and is slightly greater than the uncertainties given by the combination of experimental and ion fraction uncertainties.

The K FIP bias is very high, higher than the values quoted in the literature for the other low-FIP elements. Feldman & Laming (2000) suggest that the FIP bias for the very low-FIP elements such as K could be higher than for the normal low-FIP elements such as Mg, Si and Fe, so that the FIP effect for low-FIP elements could be dependent on the FIP itself. Feldman & Laming (2000) base their suggestion on a number of measurements, whose uncertainties however are as large as this effect itself. The present work seems to support the Feldman & Laming (2000) suggestion with new measurements from active region SUMER measurements, but it is not possible to draw any firm and definitive conclusion because of the presence of a Si VIII blending line, whose contribution to the total intensity is very difficult to determine. It is possible that the presence of this Si VIII could significantly reduce the K FIP bias to lower levels, but it is difficult to determine whether the K FIP bias is higher than, or of the order of, the FIP bias of the other low-FIP elements.

It is recommended that further studies on K lines, and more accurate and complete atomic models for the calculation of Si VIII line intensites are carried out, in order to address this problem.

The evident height dependence of the K FIP bias is a new observational fact whose magnitude (a factor around 2) is larger than the combined experimental and theoretical uncertainties. Of further interest, the Si FIP bias seems also to be dependent on height, decreasing with the distance from the solar limb. This behaviour has been already noted by Laming et al. (1999) in quiet corona; the authors suggest that this decrease with height might be due to emission from fast solar wind plasma present in the field of view. Since the fast solar wind plasma composition resembles the photospheric one, its emission would have the effect of decreasing the FIP bias of low-FIP elements with increasing height. However, the height dependence of the K FIP bias goes in the opposite direction, apparently contradicting Laming et al. (1999).

7. Conclusions

In the present work we have studied SUMER observations of a solar active region at the limb, to investigate the FIP bias in both cool plasma confined in the core of an active region, and in the more diffuse, unstructured hot corona surrounding them. We use lines from the high-FIP Ne VI, Ar XII ions, the intermediate-FIP S X ion, and from the low-FIP Mg VI, Mg VII, Si XI and K XIII ions.

We find that the Mg/Ne relative abundance is highly variable in the complex, cool core of the active region, and seems to be strongly correlated to line intensity patterns; this might suggest that each (spatially unresolved) plasma structure might have its own peculiar composition. Mg abundance enhancements relative to Ne reach up to a factor of 8.8.

The analysis of the diffuse corona seems to suggest that in off-limb active region plasma the FIP bias inside the low-FIP elements' class is dependent on the FIP value, being higher for the very-low FIP element K, although the presence of a Si VIII blending line makes this conclusion uncertain. Since FIP dependent FIP bias can provide important constraints on FIP effect models, further work is recommended on this subject.

Also, we provide some evidence of height dependence of the FIP bias for K and Si, while the S results are constant with height within the uncertainties.

References

Allen R., Landi E., Landini M., Bromage G.E., 2000, A&A 358, 332
Anders E, Grevesse N., 1989, Geochim. Cosmochim. Acta 53, 197
Arnaud M., Rothenflug R., 1985, A&AS 60, 425
Bhatia A.K., Mason H.E., 1980, MNRAS 190, 925
Brown J.C., Dwivedi B.N., Almleaky Y.M., Sweet P.A., 1991, A&A 249, 277

Delaboudiniere J.-P., Artzner G.E., Brunaud J., et al., 1995, Solar Phys. 162, 291

Dere K.P., Landi E., Mason H.E., Monsignori Fossi B.C., Young P.R., 1997, A&AS 125, 149

Doschek G.A., Feldman U., Seely J.F., 1985, MNRAS 217, 317

Dwivedi B.N., 1994, Space Sci. Rev. 65, 289

Dwivedi B.N., Mohan A., 1995, Solar Phys. 157, 135

Dwivedi B.N., Curdt W., Wilhelm K., 1997, paper presented at the JD19/IAU, Kyoto, August 26-27

Dwivedi B.N., Curdt W., Wilhelm K., 1999a, ApJ 517, 516

Dwivedi B.N., Curdt W., Wilhelm K., 1999b, ESA SP-446, 293

Feldman U., Behring W.E., Curdt W., et al., 1997, ApJS 113, 195

Feldman U., Schühle U., Widing K.G., Laming M.J., 1998, ApJ 505, 999

Feldman U., 1992, Phys. Scripta 46, 202

Feldman U., Laming J.M., 2000, Phys. Scripta 61, 222

Gianetti D., Landi E., Landini M., 2000, A&A 360, 1148

Kink I., Engström L., Feldman U., 1999, ApJ 512, 496

Klapisch M., 1971, Comput. Phys. Commun. 2, 239

Klapisch M., Schwab J.L., Fraenkel J.S., Oreg J., 1977, J. Opt. Soc. Am. 61, 148

Laming J.M., Feldman U., Drake J.J., Lemaire P., 1999, ApJ 518, 926

Landi E., Landini M., 1998a, A&A 340, 265

Landi E., Landini M., 1998b, A&AS 133, 411

Landi E., Landini M., Dere K.P., Young P.R., Mason H.E., 1999, A&AS 135, 339

Landini M., Monsignori Fossi B.C., 1991, A&AS 91, 183

Lemaire P., Wilhelm K., Curdt W., et al., 1997, Solar Phys. 170, 105

Liedahl D.A., Osterheld A.L., Goldstein W.H., 1995, ApJ 438, L115

Mason H.E., Monsignori-Fossi B.C., 1994, A&AR 6, 123

Mazzotta P., Mazzitelli G., Colafrancesco S., Vittorio N., 1998, A&AS 133, 403

Mohan A., Dwivedi B.N., Landi E., 2000, Journal of Astron. and Astroph. in press

McIntosh S.W., Brown J.C., Judge P.G., 1998, A&A 333, 333

Widing K.G., Feldman U., 1993, ApJ 416, 392

Widing K.G., Feldman U., 1995, ApJ 442, 446

Wilhelm K., Lemaire P., Curdt W., et al., 1997, Solar Phys. 170, 75

Wilhelm K., Curdt W., Marsch E., et al., 1995, Solar Phys. 162, 189

Young P.R., Mason H.E., 1997, Solar Phys. 175, 523

Zhang H.L., Sampson D.H., 1999, ADNDT 72, 153